**Structural and Multidisciplinary Optimization**
(will be inserted by the editor)

# Topology Optimization Considering Overhang Constraint under support element evaluation in additive manufacturing

**Qiaochu Ma** ·

**Abstract** Additive manufacturing (AM) makes it possible to fabricate optimized typology design concepts that have complex geometric characteristics. However, to print these complex geometric design solutions typically require additional material, energy, and time that may not be directly related to the final solution itself. For example, complex solutions that are not capable of supporting overhanging sections require support structures. A support structure is printed material that is used to support a part during the printing process, but is removed when the process is completed. The use of support structures increases the amount of material used to print a design while also requiring additional energy and time. Furthermore, the removal of support structures might be difficult due to the complexity of the design's geometry adding additional complications to the printing process. These complications can be circumvented by determining a design solution that is self-supporting. A self-supporting design solution means that supporting structures are not printed since the design can support itself. To realize a self-supporting design solution, certain manufacturing constraint are considered in the topology optimization process. Therefore, this paper considers incorporating an overhang constraint in the topology optimization process that results in a self-supporting design solution. Specifically, the constraint function is constructed based on the support element region identified by a critical overhang angle. The proposed function can be added into any density-based topology optimization formulation and solved by a common gradient-based optimizer. The proposed approach's performance and characteristics are investigated through the application of several numerical examples.

**Keywords** Topology optimization · Overhang constraint · Self-supporting structures · Additive manufacturing

Address(es) of author(s) should be given

## 1 Introduction

Additive manufacturing (AM) has been rapidly developing since the appearance of stereolithography, the first additive manufacturing (AM) technique introduced in 1987 by 3D Systems. Its development has resulted in the investigation and commerializaton of many different AM techniques and methodologies over the years (Gibson et al. 2014). Of its many unique capabilities, design flexibility is one of AM's most desirable features (Gao et al. 2015). Specifically, AM offers the opportunity to create almost any complex geometric shape, which naturally makes it pair well with topology optimization (Zegard and Paulino 2016; Ranjan et al. 2017). Therefore, to fully exploit the benefit of AM combined with topology optimization, existing designs should be redesigned with the consideration of all the unique design solutions that AM can offer (Atzeni and Salmi 2012).

Topology optimization was first proposed in 1988 by Bendsoe and Kikuchi (1988). The method introduced at that time was called the homogenization method. The general purpose of the method was to find the optimal distribution of material in a design domain, with the specific requirements associated with the applied loads, support conditions, and volume in the form of a constraint. Additional constraints could be applied depending on the application. The homogenization method was considered difficult and the resulting solutions had little benefit in manufacturing since it required the evaluation of optimal microstructures and their orientation within an element. Therefore density-based methods were proposed. Among the different density-based methods, the Solid Isotropic Material with Penalization (SIMP) approach has become the most popular topology optimization method at present (Bendsøe 1989). A detailed introduction to the SIMP method can be found in the book written by Bendsoe and Sigmund (2013).

Apart from the SIMP method, various topology optimization approaches have been proposed and improved over the years. A level set model was introduced and is suitable to describe complex topological changes, one advantage of the method is that it could define the boundaries accurately during the topology optimization process (Wang et al. 2003; Yulin and Xiaoming 2004). Also, an evolutionary based algorithm was proposed (Querin et al. 1998) and has been improved upon in the past decade (Huang and Xie 2009). A comparative review on various topology optimization methods is presented by Sigmund and Maute (2013).

Although AM reduces the amount of restrictions associated with the manufacturing, certain rules must be followed (Adam and Zimmer 2015). For example, the overhang constraint is the most universal restriction in both metal and polymer AM technologies. An overhang angle is defined by the inclination of downward facing surfaces, which is limited to a certain angle. If a section of a printed part violates the overhang constraint then additional support in the form of a support structure is required to aid in the printing process. The specified angle associated with the overhang constraint is called the critical overhang angle and can be used to identify where support structures are needed. Support structures are costly in AM because they not only require additional energy, time, and material that is simply discarded after the printing process, but also effort in their removal during in the post-processing phase (Wang et al. 2013). Specified critical angles have been extensively studied and are typically defined between 40° to 50° (Wang et al. 2013; Mertens et al. 2014; Kranz et al. 2015)

Two approaches exist that are used to address the complications associated with support structures. The first approach uses topology optimization techniques on the support structures themselves in order to minimize the support structure materials. Kuo et al. (2018) introduced a multi-objective topology optimization formulation that quantifies both the removal of support structure and the cost of support structure and then incorporates them into a support structure topology optimization process. The second approach eliminates the inclusion of the support structure whereby methods incorporates overhang limitations in the topology optimization approach (Gaynor et al. 2014). In particular, a Heaviside projection scheme is applied in the topology optimization process without adding an explicit constraint, however, convergence issues are encountered in some solutions. Furthermore, Langelaar presented a method to construct an AM filter into the toplogy optimization process (Langelaar 2017). In order to construct the AM filter, Langelaar introduced a fabrication model to evaluate the underlying layers of the design solution, which is in this work to evaluate support elements with some modifications.However, this technique does not explicitly include an overhang constraint and the AM filter has the problem of density buildup because of the Min and Max approximation. Qian (2017) introduced a density gradient based approach that is utilized with the Heaviside projection to impose the overhang angle and undercut control. Garaigordobil et al. (2018) introduced a novel method in using an edge detection technique paired with image processing to formulate the overhang constraint explicitly. Evaluation to the surrounded elements is needed for every element in the design domain, which takes extra computational time.

Inspired by Brackett et al. (2011), this paper presents an alternative approach that explicitly incorporates an overhang constraint in the conventional topology optimization process to generate an optimized self-supporting design solution. The devised overhang constraint can be readily inserted into a typical minimum compliance problem with a maximum volume fraction constraint, and it can be easily solved by traditional mathematical programming optimization algorithms. The Method of Moving Asymptotes (MMA) (Svanberg 1987) is used to derive the numerical solutions in this paper. The constraint developed in this paper refers to the ratio between the admissible relative density and inadmissible relative density with additional quality index and penalty index in order to get a crisp design. The remainder of the paper is organized as follows. In section 2 the proposed methodology pertaining to the formulation of the proposed overhang constraint based on the evaluation of the elements in a layer by layer manner that mimics the actual AM printing process is described. Furthermore a description of the sensitivity analysis used in include. Section 3 presents several numerical examples that applies the described methodology. Lastly, the main contributions and findings are summarized in Section 4.

## 2 Methodology

### 2.1 Support Element Model

The support element model in this work is based on the fabrication model introduced by Langelaar (2017). A support element model is defined as the elements in a layer below the target element and within the admissible region that is determined by a critical overhang angle, which in our work is set to be 45°. The target element has the coordinates $(i, j)$ and by considering the overhang angle three support elements are located below the target with the following coordinates: $(i-1, j-1), (i-1, j)$, and$(i-1, j+1)$. Figure 1 illustrates the set of support elements in row $i-1$ that are evaluated for target element in row $i$. The elements highlighted in light blue represent the support elements while the dark blue represents the target element.

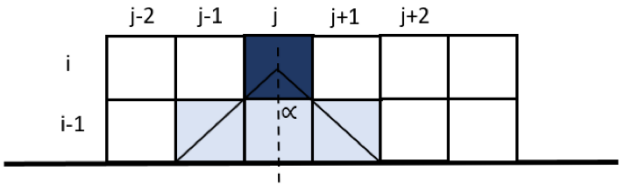


**Fig. 1** Illustration of support element model.

Formally, $P_{i,j}$ represents the set of elements that could support the target element and denoted as:

$$P_{i-1,j} = [\rho_{i-1,j-1}, \rho_{i-1,j}, \rho_{i-1,j+1}] \tag{1}$$

where $\rho$ represents the density of the each support element at the specified location denoted by its subscripts. The maximum density in $_{i,j}$ can easily be found in order to compare with the density of target element. Therefore, eqn. 2 is used to find the maximum value $\zeta_{i,j}$ in the supporting region that is supporting the element with density of $\rho_{i,j}$.

$$\zeta_{i,j} = \max(P_{i-1}) \tag{2}$$

However, in order to make the operation differentiable, a smooth maximum function is used as follows:

$$\zeta_{i,j} = \frac{\sum_{m=-n}^{n} \rho_{i-1,j} e^{\alpha \rho_{i-1,m}}}{\sum_{m=-n}^{n} e^{\alpha \rho_{i-1,m}}}, \qquad \text{n= 2} \tag{3}$$

where as $\alpha$ is smoothness parameter and as it approaches positive infinity $\zeta_{i,j}$ gives the maximum value. For this work $\alpha = 700$. The resulting approximation error can be neglected since $\zeta_{i,j}$ is not used directly in the optimization loop. The following section discusses the construction of the overhang constraint which is based on the support element model.

## 2.2 Overhang Constraint

As previously discussed, the main objective of this work is to formulate an effective and versatile overhang constraint that when added to the topology optimization process results in a self supporting design solution. Specifically a design that does not require support structures during the additive manufacturing process. Based on the overhang constraint definition, target elements that need support structures should have a density less than or equal to the maximum element density within the support element region. In order to make the comparison, the difference between the target element density and maximum support element density is determined using eqn. 4.

$$\psi_{i,j} = \rho_{i.j} - \zeta_{i,j} \tag{4}$$

where $\psi_{i,j}$ is the difference of the density related to the target element $\rho_(i,j)$ and the maximum support density $\zeta_{i,j}$. The overhang constraint for target element $\rho_{i,j}$ is violated when $\psi_{i,j} > 0$. To extend the overhang constraint formulation, the total support relative density, $S$, can be calculated by using the following:

$$S = \sum_{m=1}^{n} \max(0, \psi_{i,j}(\rho_{i,j} + \zeta_{i,j})P) \tag{5}$$

where $\rho_{i,j} + \zeta_{i,j}$ represents a weighting factor that quantifies the quality of the target element and its corresponding support element region. $P$ is the overhang penalty index that penalizes the formation of the target element that violates the overhang constraint. The default value is set to 20. The target element satisfies the overhang constraint if $\psi_{i,j} \leq 0$. The total non-support relative density, $N$, can be calculated as follows:

$$N = -\sum_{m=1}^{n} \min(0, \psi_{i,j}(\rho_{i,j} + \zeta_{i,j})) \tag{6}$$

where the relative density $\psi_{i,j}$ is multiplied by the element quality weighting factor $\rho_{i,j} + \zeta_{i,j}$ and summed up for every element that has relative density less than or equal to zero. In order to make the quantity positive, the quantity is multiplied by $-1$. By determining the percentage of total non-support relative density to overall relative density, the weight percentage of elements that do not need support structures to the overall structure can be estimated, comparing it with the desire non-support structure ratio $\psi_0$, the overhang constraint can be formulated as follow:

$$\psi_{i,j} = \psi_0 - \frac{N}{N+S} \leq 0 \tag{7}$$

where $\psi_0$ is the desired non-support structure ratio from 0 to 1. In this paper 0.97 is used. As we will see in the numerical examples, 0.97 is sufficient level to result in a self-supporting design solution. It is important to note that setting the desired ratio to 1 will create convergence issues in the optimization process.

## 2.3 Density Filter and Heaviside Projection

In order to prevent the common problems associated with the SIMP method, such as checkerboarding and mesh dependence, projection methods and density filters based on the Heaviside function are used. The use of a density filter in a topology optimization problem has been shown to be effective in reducing the SIMP method's shortcomings (Sigmund and Petersson 1998). In addition to including a density filter, projection methods are used in this work to convert density output to a binary representation. The density filter is formulated as follows:

$$\bar{\rho}_e = \frac{1}{\sum_{i \in N_e} H_{ei}} \sum_{i \in N_e} H_{ei} \rho_i \tag{8}$$

where $H_{ei}$ is a weight factor determined by the filter radius $r_{min}$ and $N_e$ is a set of elements in the domain within the filter radius for element $i$. The filter radius is defined as:

$$H_{ei} = \max(0, r_{min} - dist(e,i)) \tag{9}$$

Although the density filter solves the issues related to mesh dependency, the embedded smoothing operation implies the existence of grey areas, which makes the results hard to interpret. Therefore, a projection step is added to eliminate grey areas during the optimization process. The implementation of the projection function is introduced by Andreassen et al. (2011). In this work, a continuous approximation of the Heaviside function is used. The function is based on the hyperbolic tangent function (Wang et al. 2011). Where $\eta$ is set as a threshold parameter and any $\tilde{\rho}_e$ values below $\eta$ are projected to 0 and the values above $\eta$ are projected to 1. $\tilde{\rho}_e$ is defined as:

$$\tilde{\rho}_e = \frac{\tanh(\beta \times \eta) + \tanh(\beta \times (\bar{\rho}_e - \eta))}{\tanh(\beta \times \eta) + \tanh(\beta \times (1 - \eta))} \tag{10}$$

where $\beta$ is a scaling parameter that controls the closeness of the approximation and $\eta$ is the threshold parameter of the Heaviside function. In the optimization process, $\tilde{\rho}_e$ replaces the original design variable density $\rho_e$ and is referred to as the physical density. In other words, both the objective and constraint functions are calculated based on the physical density, rather than the original design variable density. A critical point in applying the Heaviside function to the SIMP method is that a continuous scheme must be used to avoid problems associated with the sensitivity calculation and large $\beta$ values. Also, when applying the MMA method as an optimizer, as $\beta$ gets larger, $\tilde{\rho}_e$ can oscillate dramatically making the results invalid. Therefore several adjustments were made to the original MMA formulation to make the distance of the asymptotes relate to the value of $\beta$ as proposed by Guest et al. (2011).

### 2.4 Problem Formulation and Sensitivity Analysis

This work considers the compliance minimization topology optimization formulation. In other words the task objective is to minimize the compliance which results in the stiffest design that satisfies a specified volume constraint. Unique to this work is the inclusion of the additional overhang constraint in the problem formulation. The additional constraint should result in a self-supporting design solution. Formally the problem is formulation is as follows:

$$\begin{aligned} \min \quad & c(\rho) = U^T K U = \sum_{e=1}^{N} E_e(\rho_e) u_e^T k_0 u_e \quad \textit{Compliance} \\ \text{s.t.} \quad & KU = F \qquad \textit{Equilibrium} \\ & V(\rho) \le V_0 \qquad \textit{Volume} \\ & \psi(\rho) \le V_0 \qquad \textit{Overhang} \\ & 0 \le \rho \le 1 \qquad \textit{Bounds} \end{aligned} \tag{11}$$

where $c(\rho)$ is the actual compliance in the current iteration, $U$ is the global matrix of displacement, $K$ is the global stiffness matrix, and $E_e$ is the modified Young's modulus. $u_e$ and $k_o$ are the element nodal displacement and stiffness matrix for a solid element. $F$ represents the nodal force vector. $V(\rho)$ is the actual structure volume fraction and $V_0$ is the critical structure volume fraction. $\psi(\rho)$ represents the overhang constraint introduced before.

The well known density-stiffness interpolation scheme is applied to generate the Young's modulus in order to avoid generating an $E$ equal to zero. However, the physical density is used to replace the original design variable density. The modified Young's modulus, $E_e$, is defined as:

$$E_{i,j}(\rho) = E_{min} + (E_0 - E_{min}) \partial \tilde{\rho}_{i,j}^p(\rho) \tag{12}$$

where $p$ is the penalization parameter, $E_{min}$ is the modulus of void material, which is assigned a very small number, for example $E_{min} = 10^{-9}$, and $E_0$ is the Young's modulus in the solid isotropic phase.

The formulation of the sensitivity analysis to the topology optimization begins by considering the derivatives of the functions $f(\rho)$ with respect to the original design variable density $\rho_{i,j}$ and using the chain rule to solve. Since both the Heaviside projection and density filter are used in the topology optimization, the derivative of the function $f(\rho)$ is formulated as:

$$\frac{\partial f(\rho)}{\partial \rho_{i,j}} = \frac{\partial f(\rho)}{\partial \tilde{\rho}_{i,j}} \frac{\partial \tilde{\rho}_{i,j}}{\partial \bar{\rho}_{i,j}} \frac{\partial \bar{\rho}_{i,j}}{\partial \rho_{i,j}} \tag{13}$$

where the first term in eqn. 13 is the derivative of overhang constraint with respect to the physical density, the second term is the derivative of the physical density with respect to the filtered density, and the third term is the derivative of the filtered density with respect to the original design variable density. The described derivatives are defined using the following equations:

$$\frac{\partial \tilde{\rho}_{i,j}}{\partial \bar{\rho}_{i,j}} = \frac{\beta[1 - \tanh^2(\beta \times (\bar{\rho}_{i,j} - \eta))]}{\tanh(\beta \times \eta) + \tanh(\beta \times (1 - \eta))} \tag{14}$$

$$\frac{\partial \bar{\rho}_{i,j}}{\partial \rho_{i,j}} = \frac{H_{i,j}}{\sum_{k \in N_e} H_{i,j,k}} \tag{15}$$

It can be concluded that the second and third terms in the sensitivity analysis are the same to any function. Now let us exam the first term to each function respectively. The derivative of the objective function, which is the compliance with respect to the physical density, can be calculated as follows:

$$\frac{\partial c}{\partial \tilde{\rho}_{i,j}} = -p \times (E_0 - E_{min}) \tilde{\rho}_{i,j}^{p-1} \times u_e^T k_0 e_e \tag{16}$$

The derivative of the volume constraint with respect to the physical density can be obtained using:

$$\frac{\partial V}{\partial \tilde{\rho}_{i,j}} = v_{i,j} \tag{17}$$

With the above defined, the derivative of the overhang constraint, $\psi(\rho)$ with respect to the physical density $\partial\tilde{\rho}_{i,j}$ can be solved for. The direct method is used to obtain the analytical solution and takes the following form:

$$\frac{\partial\psi}{\partial\tilde{\rho}_{i,j}} = \frac{\frac{\partial S}{\partial\tilde{\rho}_{i,j}}}{N+S} - S\frac{\frac{\partial N}{\partial\tilde{\rho}_{i,j}} + \frac{\partial S}{\partial\tilde{\rho}_{i,j}}}{(N+S)^2} \tag{18}$$

In order to derive the overhang constraint sensitivity in eqn. 18, the derivatives of the total support relative density $S$ with respect to the density $\frac{\partial S}{\partial\tilde{\rho}_{i,j}}$ and of the total non-support relative density $N$ with respect to the density $\frac{\partial N}{\partial\tilde{\rho}_{i,j}}$ were determined. To solve for $\frac{\partial S}{\partial\tilde{\rho}_{i,j}}$, each element must be considered layer by layer. For the elements in the top layer, the change in element density will only impact $\rho_{i,j}$ in formula 5. For each element in the following layers, the change on element density will not only impact $\rho_{i,j}$, but also $\zeta_{i+1,j}$ in the support element region. Equation 19 shows the derivative of $S$ with respect to $\rho_{i,j}$; eqns. 20, 21, and 22 shows the derivative of S with respect to $\zeta_{i+1,j-1}$, $\zeta_{i+1,j}$, and $\zeta_{i+1,j+1}$ respectively. Equation 23, $\frac{\partial S}{\partial\tilde{\rho}_{i,j}}$, is the sum of eqns. 19, 20, 21, and 22.

$$\frac{\partial S}{\partial\tilde{\rho}_{i,j}}(1) = \begin{cases} 0, & \Psi_{i,j} \le 0 \\ 2P\tilde{\rho}_{i,j}, & \Psi_{i,j} > 0 \end{cases} \tag{19}$$

$$\frac{\partial S}{\partial\tilde{\rho}_{i,j}}(2) = \begin{cases} 0, & \Psi_{i+1,j-1} \le 0 \\ -2P\zeta_{i+1,j-1}\frac{\partial\zeta_{i+1,j-1}}{\partial\tilde{\rho}_{i,j}}, & \Psi_{i+1,j-1} > 0 \end{cases} \tag{20}$$

$$\frac{\partial S}{\partial\tilde{\rho}_{i,j}}(3) = \begin{cases} 0, & \Psi_{i+1,j} \le 0 \\ -2P\zeta_{i+1,j}\frac{\partial\zeta_{i+1,j}}{\partial\tilde{\rho}_{i,j}}, & \Psi_{i+1,j} > 0 \end{cases} \tag{21}$$

$$\frac{\partial S}{\partial\tilde{\rho}_{i,j}}(4) = \begin{cases} 0, & \Psi_{i+1,j+1} \le 0 \\ -2P\zeta_{i+1,j+1}\frac{\partial\zeta_{i+1,j+1}}{\partial\tilde{\rho}_{i,j}}, & \Psi_{i+1,j+1} > 0 \end{cases} \tag{22}$$

$$\frac{\partial S}{\partial\tilde{\rho}_{i,j}} = \frac{\delta S}{\delta\tilde{\rho}_{i,j}}(1) + \frac{\delta S}{\delta\tilde{\rho}_{i,j}}(2) + \frac{\delta S}{\delta\tilde{\rho}_{i,j}}(3) + \frac{\delta S}{\delta\tilde{\rho}_{i,j}}(4) \tag{23}$$

It should be noted that eqns. 20, 21, and 22 will be 0 for all elements located in the top layer. For every element located at the left boundary, eqn. 20 will equal zero, and for every element at the right boundary, eqn. 22 will be equal to zero since there are no elements above that need support.

The same derivation is conducted for $\frac{\partial N}{\partial\tilde{\rho}_{i,j}}$. Equation 24 is the derivative of $N$ with respect to $\tilde{\rho}_{i,j}$; eqns. 25, 26, and 27 are the derivatives of $N$ with respect to $\zeta_{i+1,j-1}$, $\zeta_{i+1,j}$, and $\zeta_{i+1,j+1}$ respectively. Equation 28, $\frac{\partial N}{\partial\tilde{\rho}_{i,j}}$, is the sum ofeqns. 24, 25, 26, and 27.

$$\frac{\partial N}{\partial\tilde{\rho}_{i,j}}(1) = \begin{cases} 0, & \Psi_{i,j} \le 0 \\ -2\tilde{\rho}_{i,j}, & \Psi_{i,j} > 0 \end{cases} \tag{24}$$

$$\frac{\partial N}{\partial\tilde{\rho}_{i,j}}(2) = \begin{cases} 0, & \Psi_{i+1,j-1} \le 0 \\ 2\zeta_{i+1,j-1}\frac{\partial\zeta_{i+1,j-1}}{\partial\tilde{\rho}_{i,j}}, & \Psi_{i+1,j-1} > 0 \end{cases} \tag{25}$$

$$\frac{\partial N}{\partial\tilde{\rho}_{i,j}}(3) = \begin{cases} 0, & \Psi_{i+1,j} \le 0 \\ 2\zeta_{i+1,j}\frac{\partial\zeta_{i+1,j}}{\partial\tilde{\rho}_{i,j}}, & \Psi_{i+1,j} > 0 \end{cases} \tag{26}$$

$$\frac{\partial N}{\partial\tilde{\rho}_{i,j}}(4) = \begin{cases} 0, & \Psi_{i+1,j+1} \le 0 \\ 2\zeta_{i+1,j+1}\frac{\partial\zeta_{i+1,j+1}}{\partial\tilde{\rho}_{i,j}}, & \Psi_{i+1,j+1} > 0 \end{cases} \tag{27}$$

$$\frac{\partial N}{\partial\tilde{\rho}_{i,j}} = \frac{\delta N}{\delta\tilde{\rho}_{i,j}}(1) + \frac{\delta N}{\delta\tilde{\rho}_{i,j}}(2) + \frac{\delta N}{\delta\tilde{\rho}_{i,j}}(3) + \frac{\delta N}{\delta\tilde{\rho}_{i,j}}(4) \tag{28}$$

Similar to $\frac{\partial S}{\partial\tilde{\rho}_{i,j}}$, at top layer, eqns. 25, 26, and 27 will be 0, eqn. 25 is 0 for elements on the left boundary, and eqn. 27 is 0 for elements on the right boundary.

Finally the derivative of $\zeta$ with respect to $\tilde{\rho}$ can be derived. $\frac{\partial\zeta_{i,j}}{\partial\tilde{\rho}_{i,j}}$ is simply determined by taking the derivative of the smooth maximum function, as presented in the following equation:

$$\frac{\partial\zeta_{i,j}}{\partial\tilde{\rho}_{i,j}} = \frac{e^{\alpha\tilde{\rho}_{i,j}}}{\sum_{m=-n}^{n} e^{\alpha\tilde{\rho}_{i,j}}}[1+\alpha(\tilde{\rho}_{i,j}-\zeta_{i,j})], \qquad n=2 \tag{29}$$

With the derived equations in hand, sensitivities of the objective and all constraint functions can be obtained and used as inputs into the gradient based optimizer to solve the topology optimization problem. In this work, Method of Moving Asymptotes (MMA), developed by Svanberg (1987), is used as the optimizer. MMA transforms the original formulation into a set of convex functions and it is used to solve the topology optimization problems with multiple constraints efficiently.

## 3 Numerical Examples

To illustrate the functionality of the proposed optimization procedure and the characteristics of the overhang constraint parameters, several numerical examples are presented in this section. In all examples, the material properties are set to the same values, the Young's modulus $E_0 = 1$, and the lower bound $E_{min} = 10^{-9}$. The RAMP exponent p is set to be equal to 3. As mentioned previously, a 1 by 1 square mesh is used here in order to evaluate the specified 45° critical overhang angle. The continuation method is used to update the Heaviside parameter $\beta$. The Heaviside parameter $\beta$ is initially set to 1 and increased by 2 in every continuation step until a maximum value of 8 is achieved. The density filter radius is set to 1.5. Some parameters are modified and compared in the presented examples, however, by default, the overhang penalty index P is set to be 20, overhang ratio $\Psi_0$ is equal to 0.97. The volume fraction ratio is set to 0.5. The Heaviside threshold $\eta$ is set equal to 0.7. For all numerical examples, except for the cantilever beam, the design domain is discretized into 80×40 equally sized square finite elements and the

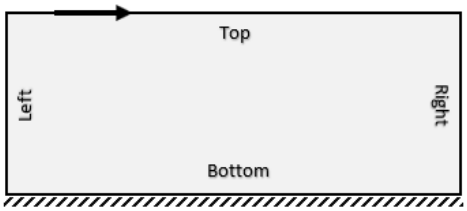


**Fig. 2** Design domain for the test case.

building orientation is set vertically from bottom to top. The reported parameters are shown to be effective and lead to accurate structural geometries. The results obtained from this work are compared with a reference result solved by the well known 88 line topology optimization MATLAB code developed by Andreassen et al. (2011), which does not include an overhang constraint.

### 3.1 Test Case

First a test case is presented to study the effectiveness of the propose topology optimization formulation with the overhang constraint. The design domain and boundary conditions are shown in Fig. 2. A single point load force is applied at the top right corner of element (1,10) while the bottom edge of the design domain is clamped and the printing direction was set from bottom to top as denoted in Fig. 2. The maximum volume fraction for the topology optimization problem is set to be equal to 0.2. The design domain was chosen to ensure that a single contour in the optimum structure is generated using the topology optimization process developed by Andreassen et al. (2011) and that this contour violates the overhang constraint.

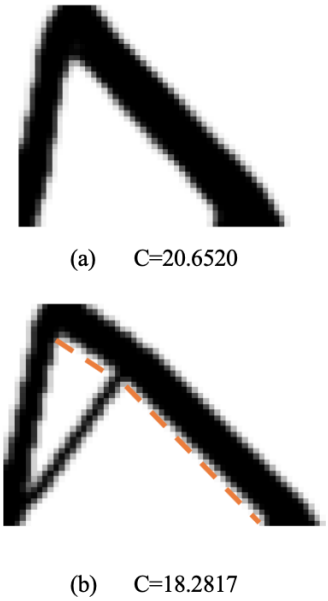

(a) C=20.6520

(b) C=18.2817

**Fig. 3** Optimum topology for the test case with (a) an overhang constraint and without (b) an overhang constraint (reference).

The described reference solution is presented in Fig. 3(b). This solution resulted from the well-known 88 lines topology optimization MATLAB code developed by Andreassen et al. (2011). The contour highlighted in orange violates the 45° overhang angle constraint thus requiring support structure during the printing process.

In comparison, the result from using this papers proposed formulation is shown in Fig. 3(a). Notably the contour that previously violated the overhang constraint in Fig. 3(b) no longer exists in the new design solution. Figure 3(a)'s design component inclinations are greater or equal to the specified 45° critical overhang angle, which validates the effectiveness of the proposed topology formulation with overhang constraint. It should be noted that the compliance increased by 2.3703 in the new design since the additional constraint is added to the topology optimization formulation.

### 3.2 MBB Beam

Now let us consider the classical MBB topology optimization problem which is defined in Fig. 4. Only half of the domain is analyzed since the beam is symmetric in geometry and loading. The lower right corner is fixed and a unit point load is vertically applied at top left corner where roller supports are assigned.

The results using this papers methodology are shown in Figs. 5(b) and 5(c), where the overhang penalty index P are 10 and 20 respectively. Compared to the reference example in Fig. 5(a), where no overhang constraint is imposed. The outer contour from of all three results is similar. However within the main structure, both Figs. 5(b) and 5(c) topologies show big differences in comparison to the reference example's in Fig. 5(a). Unlike the reference topology, the Figs. 5(b) and 5(c) topologies do not violate the overhang constraint that is imposed in their topology

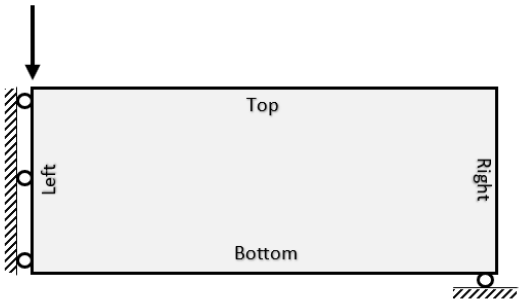


**Fig. 4** Design domain for the symmetric MBB half-case.

(a) C=85.4838

(b) C=86.8018

(c) C=84.3021

**Fig. 5** Optimum topologies for symmetric MBB beam (a) P=10 (b) P=20 (c) Reference

**Fig. 6** Optimum topology for MBB case, P=20

optimization formulation. An interesting observation is that as P increases, meaning a tighter restriction over boundaries that violate the overhang constraint, the position of the nodal locations in Fig. 5(b) move upward in Fig. 5(c) to ensure boundaries at top satisfy the overhang constraint.

In order to have a clearer picture on the optimum MBB structure, the full MBB optimum topology when P=20 is presented in Fig. 6. We can see that the outer structure does not change much when compared to the unconstrained topology. However, in order to fix the boundaries that violates overhang constraint, which are mainly focused at the upper mid of the structure, thin branch-like elements are introduced in the center of the structure to support the horizontal structures lies on the top.

To ensure a clear design solution from the proposed topology optimization formulation, the greyness of the optimum design is examined. It can be seen the solutions are black-and-white except for a small amount elements in both figures. Therefore to quantify the level of greyness (GL), the following formula was used as suggested by Sigmund (2007):

$$\text{Greyness Level} = \frac{\sum_{i=1}^{n} 4\tilde{\rho_i}(1-\tilde{\rho_i})}{n} \tag{30}$$

The GL value obtained here for the reference case in Fig. 5(a) is 0.1473 and the GL value for the result in Figs. 5(b) and 5(c) are 0.1469 and 0.1279 respectively, which are all close to the reference case and close to 0, meaning the topologies have almost 0-1 solutions as is intended by including the projection method.

The resulting topology is compared with the results from two other papers with same goal of acquiring self-support structures. Same design domain is applied in all cases, however, in our case, the domain is discretized into $80 \times 40$ meshes (Fig. 7(a)). In the paper presented by Langelaar (2017), the domain is discretized into $135 \times 45$ meshes (Fig. 7(b)), and in the paper presented by Garaigordobil et al. (2018), the domain is discretized into $165 \times 52$ meshes (Fig. 7(c)). It is well-known that finer mesh could produce better performance, meaning lower compliance in our problem. But still, our result shows lower compliance compare to the results obtained by other algorithm. The reason might due to the modification on the top contour, which eliminates some needs of supporting the ceiling that obviously violates the overhang constraint. In terms of manufacturability, Fig. 7(c) seems more favorable, since it does not have much thin struts as it has in the other two results, However, the performance is compromised, and it would be better to define other manufacturing constraints separately.

### 3.3 Bridge Structure

The following numerical example relates to a bridge problem where the design domain is shown in Fig. 8. The domain has pin supports in the lower left and right corners. A unit point load is applied vertically at the middle point of the bottom edge.

The reference design solution is presented in Fig. 9(c) and notably multiple contours violate the overhang constraint thus requiring support structure. However, in Figs. 9(a) and 9(b) the results from the proposed topology optimization algorithm result in self-supporting desings. The performance of the algorithm under different volume fraction(v) is investigated and compared against the reference design. Specifically volume constraints of 0.3 and 0.5 are investigated respectively.

In the case of 0.3 volume constraint, the overall material distribution and pattern is different to that of the reference design solution. The solution in Fig. 9(a) has thinner internal components that branch out from each other in a tree-like fashion. This is due to the fact that the process has

(a) C=86.8018

(b) C=90.2032

(c) C=95.2613

**Fig. 7** Optimum topologies comparison for MBB case, (a) Proposed algorithm (b) AM filter (Langelaar 2017) (c) SUSAN technique (Garaigordobil et al. 2018)

(a) C=26.7183

(b) C=15.3308

(c) C=14.8748

**Fig. 9** Optimum topologies for the bridge case (a) v=0.3 (b) v=0.5 (c) Reference

less volume to work with and in turn results in a higher compliance. However, the overhang constraint is satisfied.

In the case of 0.5 volume constraint, Fig. 9(b), we can see the general pattern and material distribution is not that different from the reference structure. Although the curvature of the inner boundary of the main structure gets smoother and it is no longer flat in the top- mid area, the overall pattern of how material is distributed does not change much. The alterations made satisfy the imposed overhang constraint which causes a slight increase in compliance of 3.06%. In general this means that the solution is an acceptable and valid alternative to the reference design obtained.

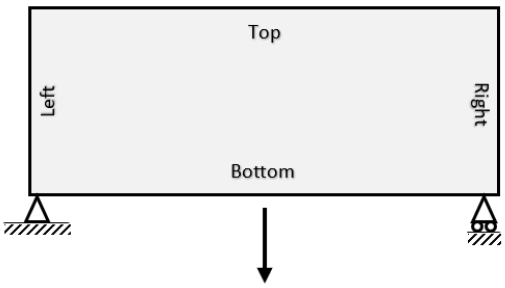


**Fig. 8** Design domain for the bridge case.

### 3.4 Cantilever Beam

Finally a cantilever beam example is considered to investigate parameter changes in the proposed algorithm. The design domain is presented in Fig. 10. The left edge is clamped and a unit point load is applied at the lower right corner of the domain.

#### 3.4.1 Overhang Constraint Parameter Influence

First we examine the parameters introduced in the overhang constraint formulation $\Psi_0$ and $P$. $\Psi_0$ is the critical non-support ratio and $P$ is the overhang penalty index. Fig. 11 presents various optimum design solutions under different combinations of $\Psi_0$ and $P$. We can see that both parameters have impact on controlling how restrictive the overhang constraint is. Increasing $\Psi_0$ closer to 1 reduces the amount of geometries that violate the overhang constraint, however, it is still not able to guarantee a completely self-supporting optimum topology that does not have a single element violating the overhang constraint. Furthermore as previously

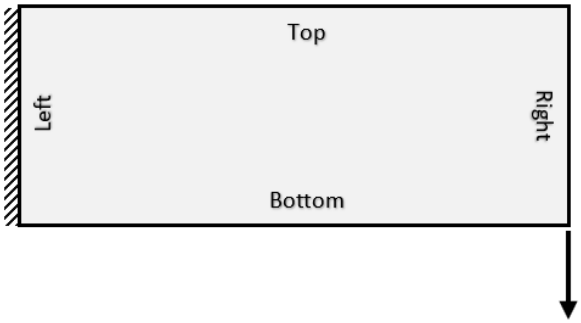


**Fig. 10** Design domain for the cantilever case.

described, $\Psi_0$ cannot be set to 1 since it will cause problems in the optimization process. However, even though a few elements might violate the overhang constraint the over design solution can still be classified as self-supporting since those elements have negligible effect on the over design.

In this work, the overhang penalty index $P$ is introduced to guarantee an acceptable self-support topology that can be obtained with a certain value of $\Psi_0$. $P$ works as a direct penalization to the relative density for elements that violate overhang constraint. As P increases, relative density for elements that violate the overhang constraint becomes larger, which results in more restrictions on the overhang constraint. $P$ gives us more control on how much of an impact the proposed constraint has on the optimization process. However, as we can see in Fig. 11, if $P$ is too large, it can lead to a design that has a much larger compliance and an increased amount of grey areas, which is not considered acceptable. It is also obvious that increasing $\Psi_0$ or $P$ would lead to a design with larger compliance in general.

#### 3.4.2 Mesh Refinement Influence

The aim of this example is to show the impact that different mesh sizes have on the resulting topology of the cantilever beam from the proposed methodology. In Fig. 12 we notice that as the mesh gets finer, the design solution changes even with the application of a density filter. This continual change is due to the nature of how the overhang constraint is defined in this work, which is the relative density between the target element density and the maximum density in the support region. When the mesh gets finer the minimum length scale gets smaller, which causes the optimization process to result in different solutions. In terms of the compliance, the design solutions get stiffer as the mesh becomes finer because the optimization process has more spaces to distribute material. In terms of the greyness, as the mesh size increases, the structure gets more well-defined. It is clearer to see that when the mesh gets finer that the thicker components in the middle of the topology contribute the most to the stiffness.

Overall, the algorithm is able to result in well defined and smaller compliance design solutions as the mesh is refined. In other words, stiffer solutions can be obtained and ultimately the results at the studied mesh sizes gives us enough detail to define the design.

#### 3.4.3 Part Orientation Influence

The purpose of this example is to examine the performance of the algorithm under different horizontal and vertical build directions. Figure 13 shows the resulting design solutions with different build directions as indicate by the blue plate. In addition, the problem is solved in the original formulation without overhang constraint for comparison.

Orientation clearly has a major impact on the optimum topologies. The overhang constraint is not violated in all the cases. In the case of orientation from top to bottom, Fig. 13(c), multiple triangular shaped voids are formed at the bottom of the support, which is a common occurrence in the study of self-support structure.

Compared to the reference case, Fig. 13(e), the build orientation from top to bottom produces the greatest compliance increase whereas the build orientation from left to right has the least increase in compliance. Therefore, the build direction from left to right is preferred for this example. For the other cases, we can see that the internal structure becomes complicated with various patterns and geometries, thus resulting in a higher compliance.

#### 3.4.4 Density Filter and Heaviside Projection Combination

This last example shows the benefit of combining both the density filter and Heaviside projection into the proposed topology optimization formulation. Without using the density filter and Heaviside projection, the checkboarding problem becomes an issue as seen in Fig. 14(a). The density filter (Sigmund and Petersson 1998) is included to address the checkerboarding problem. By including the density filter we were able to reduce the issue as seen in Fig. 14(b) but a visible amount of grey area still exist in the design solution. Therefore to reduce the amount of grey area, the Heaviside projection is used to push the intermediate density closer to 0 and 1 as discussed by Wang et al. (2011). As we can see in Fig. 14(c), most of the grey area disappears and we are left with a crisp design that does not require any further interpretation.

## 4 Summary and Closing Remarks

This paper presents a new method that incorporates the overhang limitation in AM into the density-based topology

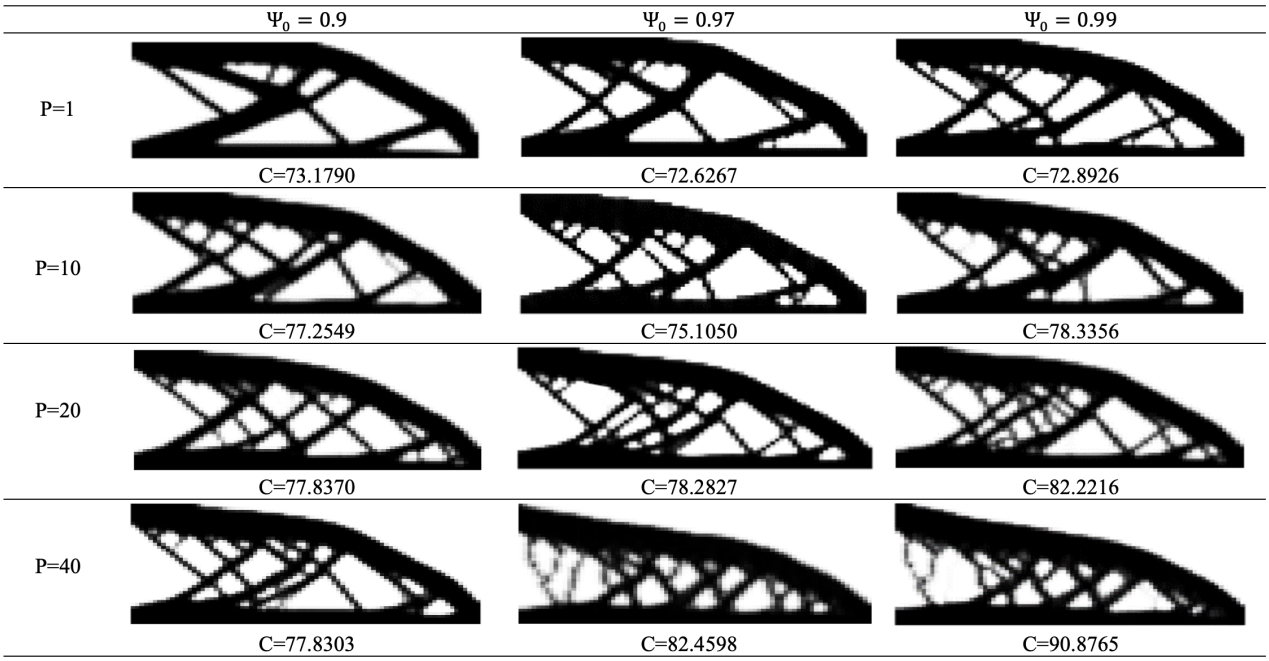


**Fig. 11** Optimum topologies for different parameters

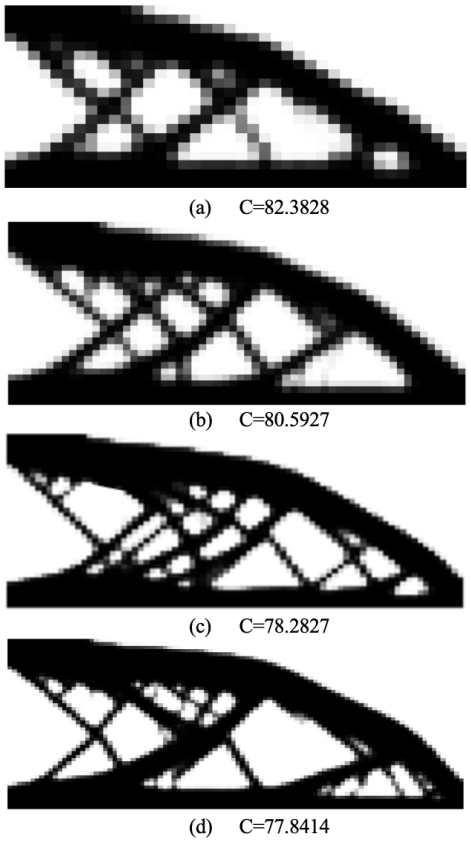


**Fig. 12** Optimum topologies for different mesh discretizations: (a) $40 \times 20$ (b) $60 \times 40$ (c) $80 \times 40$ (d) $100 \times 50$

optimization process. A self-supporting topology can be generated from the proposed algorithm without the need of further interpretation. The new features from the proposed approach include a layer by layer process in AM which is mimicked in the formation of the overhang constraint. Also, the penalty parameter introduced in the overhang constraint can control the restrictive nature of the overhang constraint. The proposed constraint can be easily added to the conventional density-based topology optimization formulation and solved by a general purpose optimizer, as seen with the MMA and the given sensitivity information presented in the paper. Common topology optimization techniques including the use of a density filter and Heaviside projection were combined with the proposed formulation in order to generate crisp design solutions.

The proposed formulation does not consider other common manufacturing limitations in AM, such as residual stresses and enclosed cavities. Also, the specified critical overhang angle was assumed to be 45° but can be varied depending on the mesh aspect ratio. Future works could include introducing more manufacturing limitations to the formulation and considering partially self-supporting design solutions.

## 5 Declarations

### 5.1 Funding

Not applicable

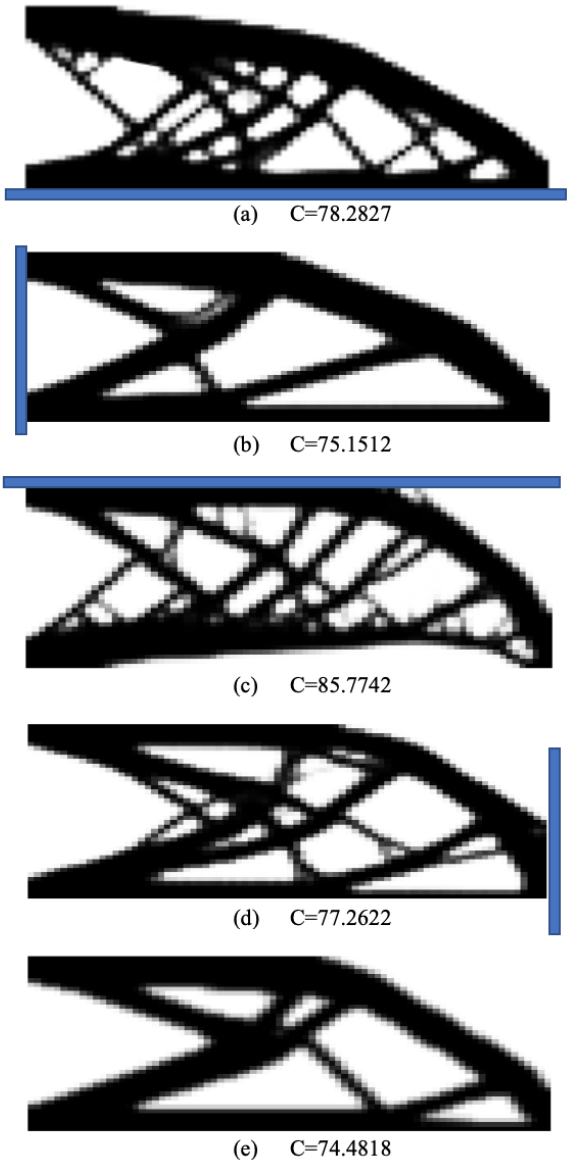


**Fig. 13** Optimum topologies for different orientation (a) bottom to top (b) left to right (c) top to bottom (d) right to left (e) reference

5.2 Conflicts of interest/Competing interests

On behalf of all authors, the corresponding author states that there is no conflict of interest.

5.3 Availability of data and material

Matlab code is available.

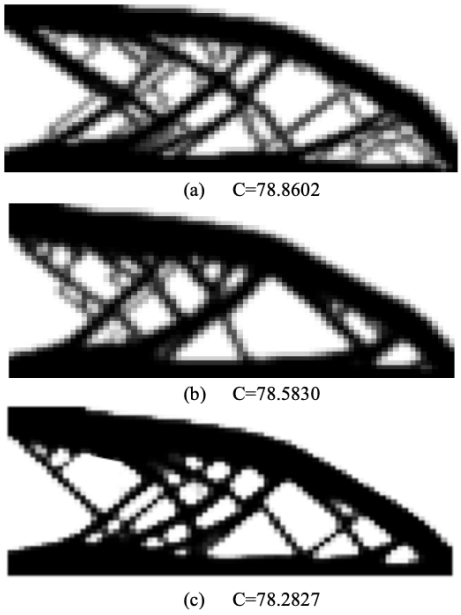


**Fig. 14** Optimum topologies for filter and HP application (a) no filter no HP (b) with filter no HP (c) with filter with HP.

5.4 Code availability

Matlab code for constructing the overhang constraint is available and will be provided in the replication of results section.

## References

Adam GA, Zimmer D (2015) On design for additive manufacturing: evaluating geometrical limitations. Rapid Prototyping Journal

Andreassen E, Clausen A, Schevenels M, Lazarov BS, Sigmund O (2011) Efficient topology optimization in matlab using 88 lines of code. Structural and Multidisciplinary Optimization 43(1):1–16

Atzeni E, Salmi A (2012) Economics of additive manufacturing for end-usable metal parts. The International Journal of Advanced Manufacturing Technology 62(9-12):1147–1155

Bendsøe MP (1989) Optimal shape design as a material distribution problem. Structural optimization 1(4):193–202

Bendsoe MP, Kikuchi N (1988) Generating optimal topologies in structural design using a homogenization method

Bendsoe MP, Sigmund O (2013) Topology optimization: theory, methods, and applications. Springer Science & Business Media

Brackett D, Ashcroft I, Hague R (2011) Topology optimization for additive manufacturing. In: Proceedings of the solid freeform fabrication symposium, Austin, TX, vol 1, pp 348–362

Gao W, Zhang Y, Ramanujan D, Ramani K, Chen Y, Williams CB, Wang CC, Shin YC, Zhang S, Zavattieri PD (2015) The status, challenges, and future of additive manufacturing in engineering. Computer-Aided Design 69:65–89

Garaigordobil A, Ansola R, Santamaría J, de Bustos IF (2018) A new overhang constraint for topology optimization of self-supporting structures in additive manufacturing. Structural and Multidisciplinary Optimization 58(5):2003–2017

Gaynor AT, Meisel NA, Williams CB, Guest JK (2014) Topology optimization for additive manufacturing: considering maximum

overhang constraint. In: 15th AIAA/ISSMO multidisciplinary analysis and optimization conference, p 2036
Gibson I, Rosen DW, Stucker B, et al. (2014) Additive manufacturing technologies, vol 17. Springer
Guest JK, Asadpoure A, Ha SH (2011) Eliminating beta-continuation from heaviside projection and density filter algorithms. Structural and Multidisciplinary Optimization 44(4):443–453
Huang X, Xie YM (2009) Bi-directional evolutionary topology optimization of continuum structures with one or multiple materials. Computational Mechanics 43(3):393
Kranz J, Herzog D, Emmelmann C (2015) Design guidelines for laser additive manufacturing of lightweight structures in tial6v4. Journal of Laser Applications 27(S1):S14,001
Kuo YH, Cheng CC, Lin YS, San CH (2018) Support structure design in additive manufacturing based on topology optimization. Structural and Multidisciplinary Optimization 57(1):183–195
Langelaar M (2017) An additive manufacturing filter for topology optimization of print-ready designs. Structural and multidisciplinary optimization 55(3):871–883
Mertens R, Clijsters S, Kempen K, Kruth JP (2014) Optimization of scan strategies in selective laser melting of aluminum parts with downfacing areas. Journal of Manufacturing Science and Engineering 136(6)
Qian X (2017) Undercut and overhang angle control in topology optimization: a density gradient based integral approach. International Journal for Numerical Methods in Engineering 111(3):247–272
Querin OM, Steven GP, Xie YM (1998) Evolutionary structural optimisation (eso) using a bidirectional algorithm. Engineering computations
Ranjan R, Samant R, Anand S (2017) Integration of design for manufacturing methods with topology optimization in additive manufacturing. Journal of Manufacturing Science and Engineering 139(6)
Sigmund O (2007) Morphology-based black and white filters for topology optimization. Structural and Multidisciplinary Optimization 33(4-5):401–424
Sigmund O, Maute K (2013) Topology optimization approaches. Structural and Multidisciplinary Optimization 48(6):1031–1055
Sigmund O, Petersson J (1998) Numerical instabilities in topology optimization: a survey on procedures dealing with checkerboards, mesh-dependencies and local minima. Structural optimization 16(1):68–75
Svanberg K (1987) The method of moving asymptotes—a new method for structural optimization. International journal for numerical methods in engineering 24(2):359–373
Wang D, Yang Y, Yi Z, Su X (2013) Research on the fabricating quality optimization of the overhanging surface in slm process. The International Journal of Advanced Manufacturing Technology 65(9-12):1471–1484
Wang F, Lazarov BS, Sigmund O (2011) On projection methods, convergence and robust formulations in topology optimization. Structural and Multidisciplinary Optimization 43(6):767–784
Wang MY, Wang X, Guo D (2003) A level set method for structural topology optimization. Computer methods in applied mechanics and engineering 192(1-2):227–246
Yulin M, Xiaoming W (2004) A level set method for structural topology optimization and its applications. Advances in Engineering software 35(7):415–441
Zegard T, Paulino GH (2016) Bridging topology optimization and additive manufacturing. Structural and Multidisciplinary Optimization 53(1):175–192

## 6 Replication of results

The Matlab code that takes the design variables and overhang penalty index as input and provide the corresponding overhang constraint value and its derivatives with respect to the design variables is available and is provided as follow:

```
function [OverhangC,doc_dx1] = overhang(x,P1)
%%rotation
rotate=0;
%bottomtotop  rotate=0
%lefttoright  rotate=1
%toptobottom  rotate=2
%righttoleft  rotate=3
x=rot90(x,rotate);
%%Preparation&Base density calculation
R=0.97; %constraint critical rate
si=size(x);%compute size of the design domain [row column]
%%Prepare xi domain for analysis
xi=zeros(si(1)+1, si(2)+4);
xi(end,:)=ones(1,si(2)+4);
for i = 1:si(1)
for j=3:si(2)+2
xi(i,j)=x(i,j-2);
end
end
%%Calculate maximum density of base elements
N=700;
for i=1:si(1)
for j=3:si(2)+2
m=i+1;
for n = j-2:j+2
yy(n)=xi(m,n);%record base element density
end
yg(i,j-2)=(yy(j-1)*exp(N*yy(j-1))+yy(j)*exp(N*yy(j))+yy(j+1)*exp(N*yy(j+1)))/(exp(N*yy(j-1))+exp(N*yy(j))+exp(N*yy(j+1)));
end
end
%% Calculate OC
Phi=zeros(si(1),si(2));Sup=0;N0_sup=0;
for i=1:si(1)
for j=1:si(2)
Phi(i,j)=x(i,j)-yg(i,j);
if Phi(i,j)>0
Sup=Sup+Phi(i,j)*(yg(i,j)+x(i,j))*P1;
else
N0_sup=N0_sup-Phi(i,j)*(yg(i,j)+x(i,j));
```

```
end
end
end
OverhangC=R-N0_sup/(Sup+N0_sup);
%% Sensitivity analysis
dNdx=zeros(si(1),si(2));dSdx=zeros(si(1),si(2));
for o=1:si(1)
for p=3:si(2)+2
if o==1
if Phi(o,p-2)>0
dxyg(o,p-2)=P1*2*x(o,p-2);
dNdx(o,p-2)=dNdx(o,p-2)+dxyg(o,p-2);
else
dxyg(o,p-2)=-1*(2*x(o,p-2));
dSdx(o,p-2)=dxyg(o,p-2);
end
else
for i=p-2:p+2
dy(i)=xi(o,i);%record base element density
end
yg1(o,p-2)=(dy(p-2)*exp(N*dy(p-2))+dy(p-1)*exp(N*dy(p-1))+dy(p)*exp(N*dy(p)))/(exp(N*dy(p-2))+exp(N*dy(p-1))+exp(N*dy(p)));
dyg1(o,p-2)=(exp(N*dy(p))*(1+N*(dy(p)-yg1(o,p-2))))/(exp(N*dy(p-2))+exp(N*dy(p-1))+exp(N*dy(p)));
yg2(o,p-2)=(dy(p-1)*exp(N*dy(p-1))+dy(p)*exp(N*dy(p))+dy(p+1)*exp(N*dy(p+1)))/(exp(N*dy(p-1))+exp(N*dy(p))+exp(N*dy(p+1)));
dyg2(o,p-2)=(exp(N*dy(p))*(1+N*(dy(p)-yg2(o,p-2))))/(exp(N*dy(p-1))+exp(N*dy(p))+exp(N*dy(p+1)));
yg3(o,p-2)=(dy(p)*exp(N*dy(p))+dy(p+1)*exp(N*dy(p+1))+dy(p+2)*exp(N*dy(p+2)))/(exp(N*dy(p))+exp(N*dy(p+1))+exp(N*dy(p+2)));
dyg3(o,p-2)=(exp(N*dy(p))*(1+N*(dy(p)-yg3(o,p-2))))/(exp(N*dy(p))+exp(N*dy(p+1))+exp(N*dy(p+2)));
if p==3
dyg1(o,p-2)=0;
if Phi(o-1,p-2)>0
dyg2(o,p-2)=-P1*2*yg2(o,p-2)*dyg2(o,p-2);
dNdx(o,p-2)=dNdx(o,p-2)+dyg2(o,p-2);
else
dyg2(o,p-2)=-(-2*yg2(o,p-2)*dyg2(o,p-2));
dSdx(o,p-2)=dSdx(o,p-2)+dyg2(o,p-2);
end
if Phi(o-1,p-1)>0
dyg3(o,p-2)=-P1*2*yg2(o,p-2)*(dyg3(o,p-2));
dNdx(o,p-2)=dNdx(o,p-2)+dyg3(o,p-2);
else
dyg3(o,p-2)=-(-2*yg3(o,p-2)*dyg3(o,p-2));
dSdx(o,p-2)=dSdx(o,p-2)+dyg3(o,p-2);
end
elseif p==si(2)+2
dyg3(o,p-2)=0;
if Phi(o-1,p-2)>0
dyg2(o,p-2)=-P1*2*yg2(o,p-2)*(dyg2(o,p-2));
dNdx(o,p-2)=dNdx(o,p-2)+dyg2(o,p-2);
else
dyg2(o,p-2)=-(-2*yg2(o,p-2)*dyg2(o,p-2));
dSdx(o,p-2)=dSdx(o,p-2)+dyg2(o,p-2);
end
if Phi(o-1,p-3)>0
dyg1(o,p-2)=-P1*2*yg2(o,p-2)*(dyg1(o,p-2));
dNdx(o,p-2)=dNdx(o,p-2)+dyg1(o,p-2);
else
dyg1(o,p-2)=-(-2*yg1(o,p-2)*dyg1(o,p-2));
dSdx(o,p-2)=dSdx(o,p-2)+dyg1(o,p-2);
end
else
if Phi(o-1,p-2)>0
dyg2(o,p-2)=-P1*2*yg2(o,p-2)*(dyg2(o,p-2));
dNdx(o,p-2)=dNdx(o,p-2)+dyg2(o,p-2);
else
dyg2(o,p-2)=-(-2*yg2(o,p-2)*dyg2(o,p-2));
dSdx(o,p-2)=dSdx(o,p-2)+dyg2(o,p-2);
end
if Phi(o-1,p-1)>0
dyg3(o,p-2)=-P1*2*yg2(o,p-2)*(dyg3(o,p-2));
dNdx(o,p-2)=dNdx(o,p-2)+dyg3(o,p-2);
else
dyg3(o,p-2)=-(-2*yg3(o,p-2)*dyg3(o,p-2));
dSdx(o,p-2)=dSdx(o,p-2)+dyg3(o,p-2);
end
if Phi(o-1,p-3)>0
dyg1(o,p-2)=-P1*2*yg2(o,p-2)*(dyg1(o,p-2));
dNdx(o,p-2)=dNdx(o,p-2)+dyg1(o,p-2);
```

```
116 else
117 dyg1(o,p-2)=-(-2*yg1(o,p-2)*dyg1(o,p-2)
        );
118 dSdx(o,p-2)=dSdx(o,p-2)+dyg1(o,p-2);
119 end
120 end
121 if  Phi(o,p-2)>0
122 dNdx(o,p-2)=dNdx(o,p-2)+P1*2*x(o,p-2);
123 else
124 dSdx(o,p-2)=dSdx(o,p-2)+(-1*(2*x(o,p-2)
        ));
125 end
126 end
127 doc_dx1(o,p-2)=dNdx(o,p-2)/(N0_sup+Sup)
        -(dNdx(o,p-2)+dSdx(o,p-2))*Sup/(
        N0_sup+Sup)^2;
128 end
129 end
130 doc_dx1=rot90(doc_dx1,-rotate);
```